Am J Nucl Med Mol Imaging 2024;14(1):48-62
www.ajnmmi.us /ISSN:2160-8407/ajnmmi0154938

Review Article

Two decades of [^{11}C]PiB synthesis, 2003-2023: a review

Paul Josef Myburgh[1], Kiran Kumar Solingapuram Sai[1,2]

[1]*Translational Imaging Program, Wake Forest School of Medicine, Winston-Salem, NC 27157, USA;* [2]*Department of Radiology, Wake Forest School of Medicine, Winston-Salem, NC 27157, USA*

Received December 13, 2023; Accepted February 4, 2024; Epub February 20, 2024; Published February 28, 2024

Abstract: Because carbon-11 (^{11}C) radiotracers cannot be shipped over long distances, their use in routine positron emission tomography (PET) studies is dependent on the production capabilities of individual radiochemistry laboratories. Since 2003, ^{11}C-labeled Pittsburgh compound B ([^{11}C]PiB) has been the gold standard PET radiotracer for *in vivo* imaging of amyloid β (Aβ) plaques. For more than two decades, researchers have been working to develop faster, higher-yielding, more robust, and optimized production methods with higher radiochemical yields for various imaging applications. This review evaluates progress in [^{11}C]PiB radiochemistry. An introductory overview assesses how it has been applied in clinical neurologic imaging research. We examine the varying approaches reported for radiolabeling, purification, extraction, and formulation. Further considerations for QC methods, regulatory considerations, and optimizations were also discussed.

Keywords: Alzheimer's disease (AD), positron emission tomography (PET), ^{11}C-tracer, [^{11}C]PiB, clinical radiochemistry

Introduction

Alzheimer's disease (AD) is the most common neurodegenerative disorder associated with progressive memory loss and cognitive impairment AD is linked to the majority of dementia cases [1, 2]. Globally, AD care provision was estimated to be over $600bn USD per annum worldwide [2].

Amyloidal plaques have been identified as a biomarker for AD in the brain [3]. Amyloid plaques are strings of amino acids known as amyloid-β (Aβ) peptides, having a common length of 40 or 42 [4, 5]. $A\beta_{42}$ is far more prevalent in AD patients than in healthy individuals and tends to aggregate together and eventually forms larger β-pleated sheet [5]. These Aβ proteins can aggregate to form different shapes and patterns [4, 6]. These Aβ aggregates have been shown to precede the onset of neurodegenerative symptoms by several years [7]. Thus, the ability to selectively image Aβ plaques could enable early diagnosis and risk prediction for AD prevalent individuals [8, 9], there are a number of studies that demonstrate the feasibility of early AD diagnosis [10-13] which would also allow patients and caregivers to be better prepared.

[^{11}C]PiB was the first broadly applied radiotracer with specificity for Aβ aggregates in humans. It has a high affinity and selectivity for Aβ plaques and other Aβ containing lesions [14]. PiB is an analog of thioflavin-T, a dye used for staining amyloid in brain tissue [15].

Mathis et al. first reported [^{11}C]PiB in 2003, as part of a preclinical evaluation of structurally similar compounds built on a 2-arylbenzothiazole backbone, abbreviated as [^{11}C]6-OH-BTA-1 and also known as [^{11}C]N-methyl-2-(4'-methylaminophenyl)-6-hydroxybenzothiazole [16]. The first clinical [^{11}C]PiB PET study with was published a year later; the radiotracer provided quantitative information on Aβ plaques in 25 participants [15]. It is now regarded as the gold standard for Aβ plaque PET [2, 17].

Radiopharmaceutical synthesis requires specialized equipment such as a cyclotron, hot cell, an automated radiochemistry module, preparative high-performance liquid chromatography (HPLC), radiation detectors, and a sterile (ISO 5) environment for peripheral use [18]. Several challenges impede commercialization of ^{11}C-radiotracers; the most prominent is the short half-life of radioactive decay ($T_{1/2}$ = 20.4 min) necessitating onsite radiosynthesis (refer to **Figure 1**). The most significant optimizations have focused on improving yield, shortening the radiochemistry duration or circumventing a step altogether minimizing points for failure and reducing reaction time. From a radiochemistry and automation point of view, fewer synthesis steps will facilitate automation and reduce potential failure points [19-21].

Optimizations reported in the literature

Molar activity (MA) or specific activity (SA) is expressed as the ratio of radioactivity (GBq) per amount of tracer or compound (μmol or μg respectively) and are thus interchangeable units. ^{11}C decays exponentially, leading to a drastic loss of activity and thus, MA over time [22]. Generally, the entire radiotracer synthesis and QC process should take no longer than 60 minutes to avoid low counts on the PET scanner that can result in noisy data [22]. Thus, shortening the total synthesis time and optimizing the QC and release processes significantly increases MA at the injection time [23]. Further, isotopic dilution

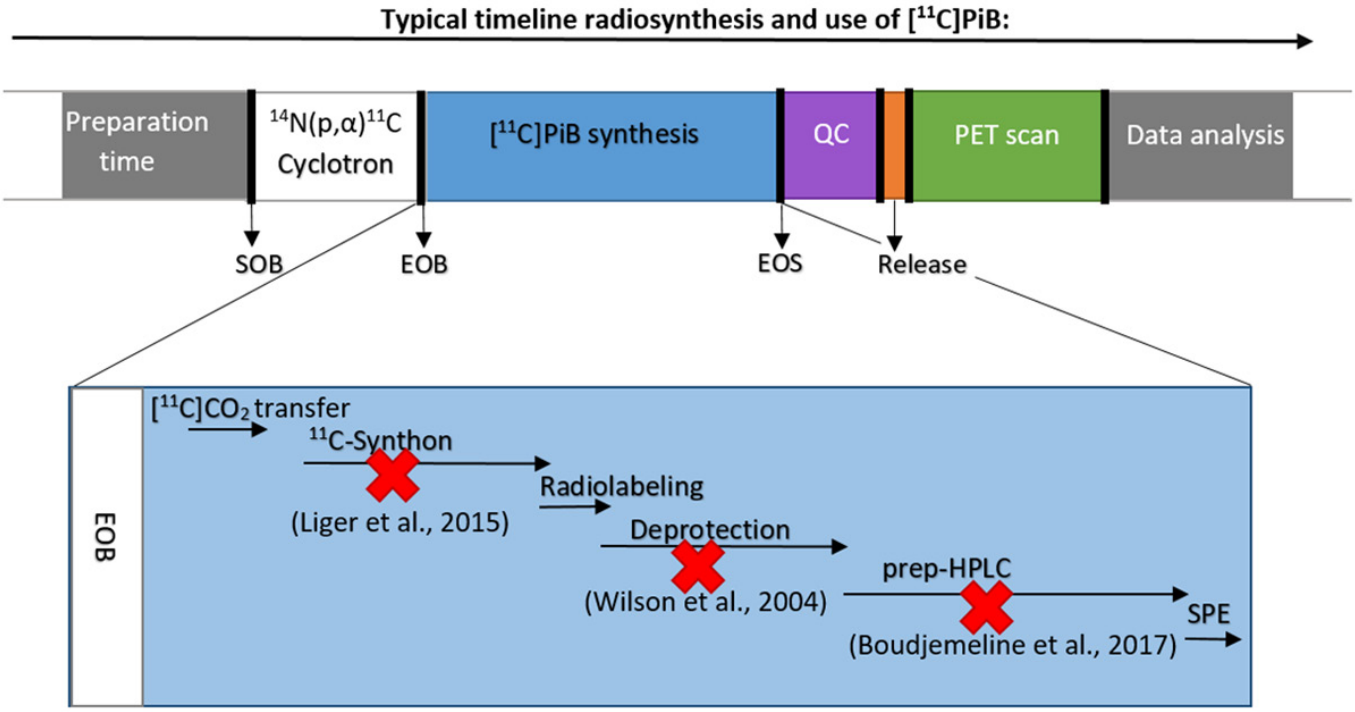

Figure 1. Typical timeline of [11C]PiB radiosynthesis. The image shows a simplified timeline of how [11C]PiB is produced and highlights important time stamps. The extended portion of PiB synthesis shows each step, such as the radiolabeling and HPLC steps. References of step removing optimizations are quoted.

of the ^{11}C-compound with a "cold" carbon-12 equivalent during the radiolabeling procedure or synthon generation would decrease MA. While isotopic dilution of [^{11}C]CO_2 with atmospheric CO_2 is hard to avoid [19], other synthesis pathways for example starting with [^{11}C]CH_4 are far easier to keep isotopically pure. "Cold" methane would have to be introduced into the system for isotopic dilution to occur [20, 24]. A higher MA improves the images quality of the eventual PET scan and has an impact on subject safety [25, 26] and can vary between production sites [25].

In this review, we evaluate progressive optimizations of [^{11}C]PiB radiochemistry. We report different published approaches on all critical aspects including radiolabeling, purification, and formulation. Further, we discussed the QC requirements and regulatory guidelines in clinical research.

Literature review

Radiolabeling pathways

The literature reports three general radiolabeling reactions (**Figure 2**) for [^{11}C]PiB, employing either *N*-methylation agents [^{11}C]methyl Iodide ([^{11}C]MeI); [^{11}C]methyltrifluoromethanesulfonate ([^{11}C]MeOTf); or alternatively [^{11}C]CO_2 fixation-reduction, depending on the auto synthesis unit and the desired level of radioactivity [27]. The original [^{11}C]PiB synthesis method used [^{11}C]MeI as the synthon; a methoxymethyl-protected alcohol group on the precursor was later removed through acid hydrolysis [16]. The second approach used [^{11}C]MeOTf as the methylation agent, eliminating the need for deprotection and significantly reducing the required synthesis time, while improving the overall radiochemical yield [28]. More than a decade passed before a third radiolabeling pathway for [^{11}C]PiB synthesis was reported, using [^{11}C]CO_2 in a one-pot catalyzed reaction [19].

^{11}C-N-methylation synthesis pathways: Through proton bombardment of N_2 gas resulting in ^{14}N(p,α)^{11}C nuclear reaction, a cyclotron can produce [^{11}C]CO_2 or [^{11}C]CH_4 based on the amount of O_2 (0.5-1%) or H_2 (5-10%), respectively, introduced into the bombardment cell. Target-produced [^{11}C]CH_4 has very high specific activity compared to target-produced [^{11}C]CO_2, which is later reduced to [^{11}C]CH_4 [20]. Oxygen and other radio impurities can be removed using a cryogenic trap (liquid nitrogen) in combination with molecular sieves prior to the radiosynthesis procedure [29, 30]. Cyclotron-produced [^{11}C]CO_2 [31] and [^{11}C]CH_4 [24] have both been used for [^{11}C]PiB radiosynthesis.

[^{11}C]MeI is an established starting material in the production of ^{11}C labeled tracers [32-34] and it has been used for [^{11}C]PiB radiolabeling both directly [16] and as an intermediate [30, 31, 35]. The longstanding "wet" method for [^{11}C]MeI synthesis involves $LiAlH_4$ dissolved in tetrahydrofuran (THF) reacted with [^{11}C]CO_2 bubbling, resulting in [^{11}C]MeO^-/[^{11}C]MeOH which was then reacted with hydroidic acid (HI) to yield [^{11}C]MeI [33]. The inherent

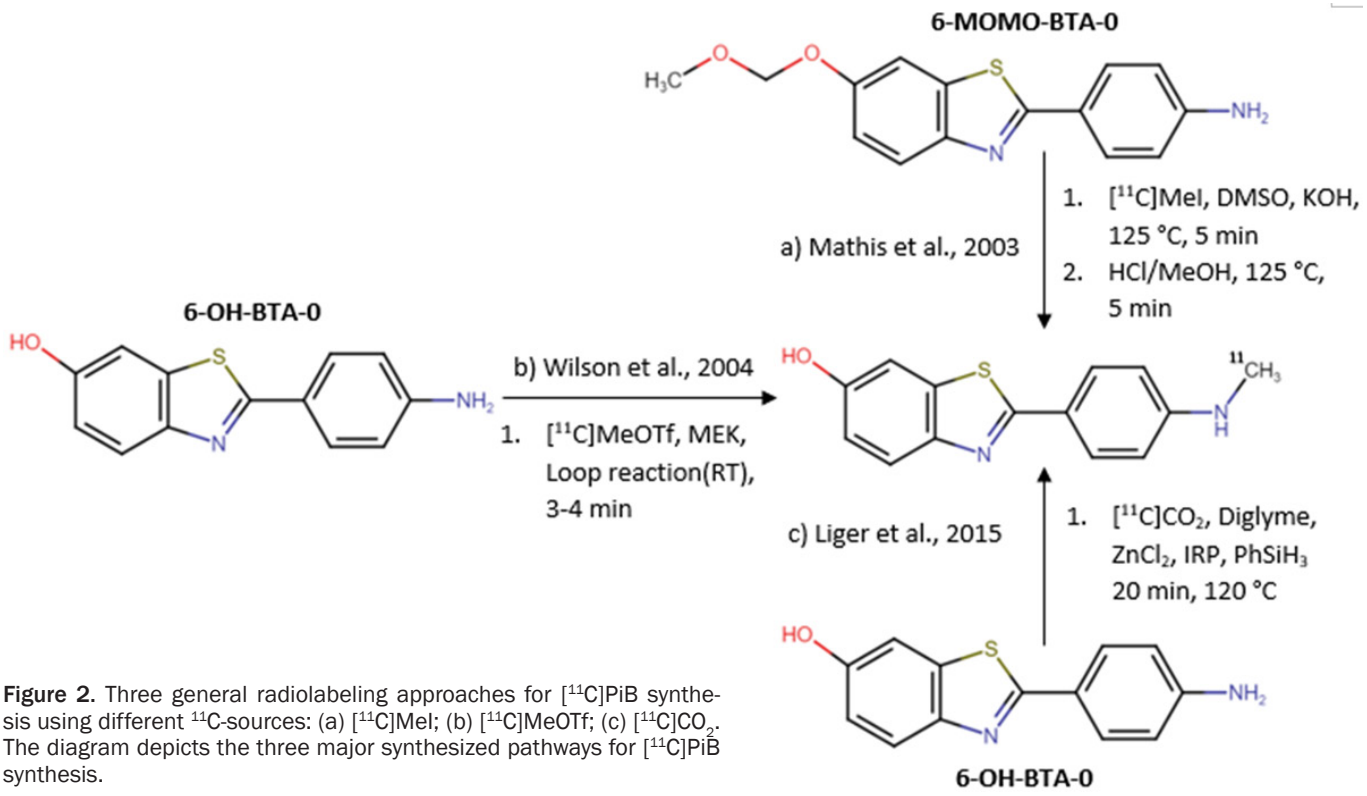

Figure 2. Three general radiolabeling approaches for [^{11}C]PiB synthesis using different ^{11}C-sources: (a) [^{11}C]MeI; (b) [^{11}C]MeOTf; (c) [^{11}C]CO_2. The diagram depicts the three major synthesized pathways for [^{11}C]PiB synthesis.

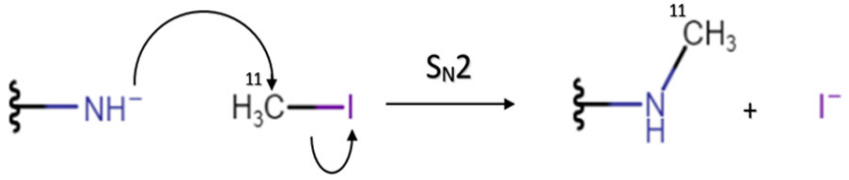

Figure 3. A proposed SN_2 reaction mechanism for the radio methylation of the primary amine of 6-MOMO-BTA-0, which acts as a nucleophile under basic conditions.

drawback to the "wet method" is the fact that the $LiAlH_4$ solution can be a source of carbon-12 isotopic dilution, considerably lowering the MA of the final [^{11}C]PiB (with MA typically ranging 50-150 GBq/μmol) [20]. Still, in the original [^{11}C]PiB synthesis, the "wet" method was used to produce [^{11}C]MeI and the reported 210 GBq/μmol is among the higher MA's in the review [16]. Despite the "wet method" producing higher radiochemical yields an unidentified radiochemical impurity co-eluting with [^{11}C]PiB during SPE purification was identified. Boudjemeline et al. suspected a double methylation byproduct might form. Such an unidentified radiochemical impurity co-eluting with [^{11}C]PiB would make clinical radiotracer batches unsuitable for imaging applications without the use of prep-HPLC. The formation of this unidentified radiochemical purity was resolved by producing [^{11}C]MeOTf separately, using the gas method, and transferring it to the employed kit. The specific activity was also improved when using the gas method over the wet method for [^{11}C]MeOTf production [35]. Note that our group reported a clinically-viable high-quality [^{11}C]PiB wet method with adequate specific activity and purity [36].

Gas phase [^{11}C]MeI synthesis results in a MA, exceeding 300 GBq/μmol, although it presents significant technical challenges [20]. A typical method for [^{11}C]MeI production involves gas phase halogenation of [^{11}C]CH_4 with iodine. In short, the cyclotron-produced [^{11}C]CO_2 was first trapped on 4 Å molecular sieve for purification. It was then reacted with hydrogen at 350-360°C under a Shimalite nickel catalyst to yield [^{11}C]CH_4, and was collected on a liquid nitrogen cooled Porapak N trap. A phosphorus pentoxide trap was required to remove impurities formed during proton bombardment and subsequent catalytic reactions. Next, the [^{11}C]CH_4 was desorbed through heating and pushed with helium through a quartz tube where the gases are mixed with vapors from iodine crystals. Heated to 60°C, the mixture was then pushed to a reaction chamber at 720 to 725°C with helium flow. The gas mixture then passed through a room-temperature quartz tube where most of the excess iodine crystallizes. An additional ascarite trap was used to remove the rest of the iodine. The resulting [^{11}C]MeI was trapped on the Porapak N trap at room temperature, and any unreacted [^{11}C]CH_4 was recirculated through the ovens for further [^{11}C]MeI synthesis. [^{11}C]MeI was desorbed from the Porapak N trap through heating to 190°C and helium carrier gas [27, 32]. This method has also been deployed with [^{11}C]CH_4 produced directly from the cyclotron [32]. When [^{11}C]CH_4 from the target and a single pass iodination procedure is used, specific radioactivity as high as 4700 GBq/μmol has been reported [20, 37]. Choosing between the wet and gas phase methods

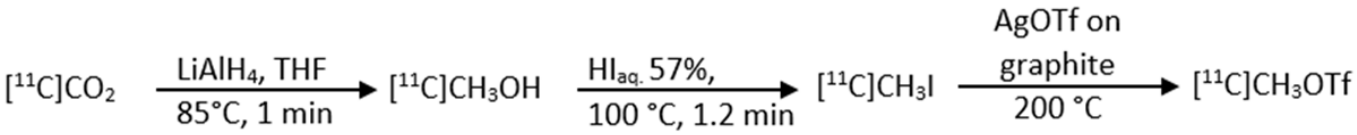

Figure 4. [11C]MeOTf preparation after [11C]MeI synthesis using the wet method [36]. An example reaction where [11C]MeOTf was prepared from [11C]MeI.

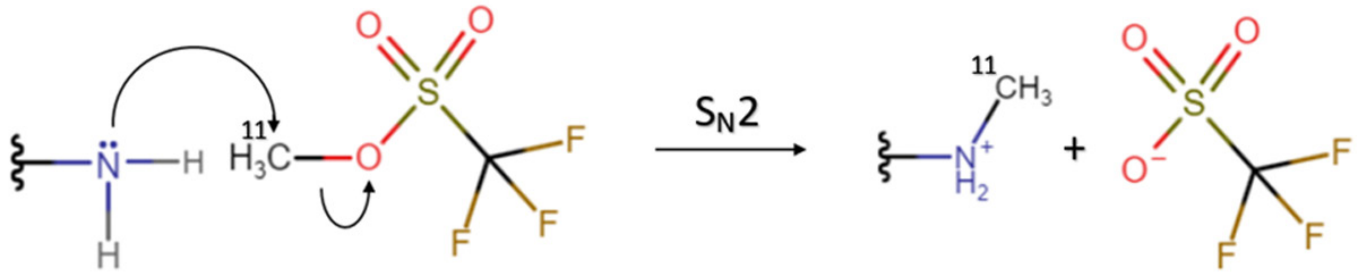

Figure 5. A proposed SN_2 reaction mechanism for N-alkylation radio methylation of the primary amine of 6-OH-BTA-0, which acts as a nucleophile.

for [11C]MeI synthesis is a tradeoff, as the wet method typically has a higher radiochemical yield [37].

Strong alkaline conditions are required to "activate" the precursor for methylation with [11C]MeI [16]. Under such alkaline conditions the primary amine was probably negatively charged leading to the reaction mechanism proposed in **Figure 3**.

[11C]MeOTf activity was trapped in the reaction vial loaded with the corresponding precursor, after [11C]MeI was passed through a column containing graphitized carbon impregnated with 50% weight silver triflate heated to 200°C, refer to **Figure 4** [27, 38]. With increasing demand for new radiotracers, [11C]MeOTf became one of the two primary [11C]synthons, along with [11C]MeI [39], and it is still widely used for novel 11C-tracer clinical applications [40]. Moreover, with higher reactivity, lower volatility, and shorter reaction times [11C]MeOTf greatly improves [11C]PiB radiochemical yields. Lower radiolabeling temperatures are required because [11C]MeOTf is a stronger methylation agent than to [11C]MeI, by a factor of ~10^4. It can readily radiolabel compounds in cases where [11C]MeI yield would be insufficient [39, 41]. Further, *N*-alkylation was so strongly dominated over *O*-alkylation with [11C]MeOTf that the protection group of 6-MOMO-BTA-0 was no longer required [28]. **Figure 5** depicts a proposed reaction mechanism for 11C-*N*-methylation using [11C]MeOTf.

The graphitized carbon impregnated with silver triflate was prepared by dissolving 1 g of silver trifluoromethanesulfonate in 150 mL of anhydrous diethyl ether. After adding 2 g of Graph-pack C (C80/100 mesh), the solution was stirred under vacuum in the dark. When ether evaporates, the resulting powder was dried under vacuum (0.2 Torr) for at least 2 more hours then stored in amber glass containers [27]. Alternatively, the reagent can be purchased from ABX-Advanced Biochemical Compounds [27].

[11C]CO_2 fixation-reduction: [11C]CO_2 is an attractive starting material for radiolabeling as it is produced directly from the cyclotron. Using [11C]CO_2 as a C_1 building block for the methylation of amines in [11C]PiB synthesis has been reported twice [17, 19]. Despite its desirable characteristics, very few studies have used this synthetic pathway in a clinical setting [40].

The catalysts used for CO_2 fixation were originally developed for carbon recycling or capture [42]. CO_2 hydrogenation usually requires metal catalysts and high temperature and pressure, but the authors report an alternative organocatalytic reaction using silane as the reductant and nitrogen base as catalysts [42]. In another study, a series of zinc catalysts to facilitate *N*-methylamine synthesis using CO_2 as a C_1 building block were reported [43]. One of the reported catalysts, $ZnCl_2$, was used to synthesize [11C]PiB directly from [11C]CO_2 [19]. **Figure 6** illustrates similarities with the methylation pathways, shown in **Figures 3** and **5**.

Another group later reported using milder reaction conditions and an organic $PhSiH_3$/TBAF catalyst mixture to achieve [11C]CO_2 fixation-reduction for [11C]PiB radiolabeling [17].

Radiolabeling strategies: There have been several reaction conditions and methodologies reported in literature for [11C]PiB synthesis. **Table 1** summarizes findings for [11C]PiB synthesis reported including reaction conditions i.e., temperatures, solvents, and reaction times with their associated yields in chronological order of publication.

Reporting yields in **Table 1** was a little challenging as some yields were reported decay corrected, and some as

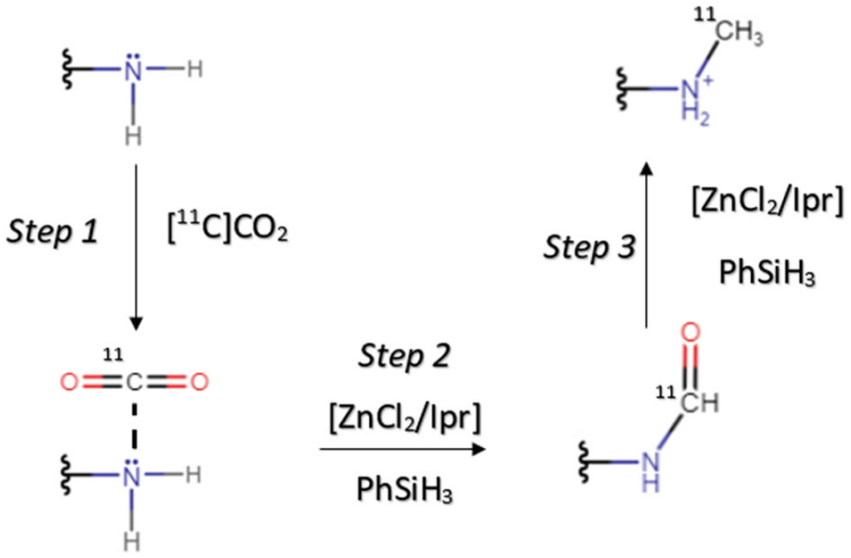

Figure 6. Hypothesized reaction steps facilitating $[^{11}C]CO_2$ fixation-reduction of the primary amine of 6-OH-BTA-0 (adapted from Liger et al. [19]).

percentages of the synthon, either [11C]MeI or [11C]MeOTf, whereas others are reported non decay corrected from the cyclotron-produced $[^{11}C]CO_2$. **Table 1** further includes the reported MA for each procedure; showing no strong correlation with any particular synthesis method. For example, the loop reactions have MA ranging from 20-265.5 GBq/μmol. Note for **Table 1** that if the alcohol group on the precursor was protected with a methoxymethyl (6-MOMO BTA-0 + [11C]MeI reaction) an additional acidic deprotection step was required [16]. Shao et al. reported a MA value of 7177 Ci/μmol; we corrected this evident misprint to 7.177 Ci/μmol as this value would have been three orders of magnitude higher than all the other reported MA values [44]. The yield of Nair et al. was calculated to report in **Table 1**, based on the reported values of 3547 MBq average product and 33-37 GBq as the typical output of [11C]MeOTf [26]. **Figure 7** displays a simplified flow diagram of all the [11C]PiB synthetic pathways reported.

Automation of [11C]PiB synthesis: Since the original [11C]PiB synthesis was performed in a V-vial heated with an oil bath (125°C) two decades ago [16], research has driven toward full automation of radiochemistry. Cheung and Ho reported a non-commercial, in-house automated apparatus for remotely operated [11C]carboxylation and bubbling [11C]methylation procedures, including [11C]PiB synthesis [45]. The automatic synthesis module, Tracer Lab FX-C Pro (GeneralElectric) can convert $[^{11}C]CO_2$ to [11C]MeI through the gas-phase reaction. It then produces [11C]CH_3OTf and facilitates the ^{11}C-*N*-methylation radiolabeling reaction and SPE (Sep Pak elution) reformulation. Although two FXC-Pro studies used another supplier's semi preparative-HPLC system, they were still controlled by the same FX-C software package [27, 44]. A fully-automated $[^{11}C]CO_2$ fixation-reduction radiosynthesis procedure was carried out using a TRACERlab® FX C PRO module from GE Healthcare, thus successfully circumventing the need to produce [11C]MeI or [11C]MeOTf before radiolabeling [17].

Clemente et al. 2012 reported an automated [11C]PiB radiosynthesis combining three Bioscan systems, $[^{11}C]CO_2$ conversion to [11C]MeI used the wet method and subsequently, [11C]MeOTf synthesis. They then used the loop method for radiolabeling and semi preparative HPLC purification [31].

A recent trend in the automation of PET radiochemistry uses cassette-based kits for production of various radiotracers on the same module with few technical modifications between syntheses [35]. Further, these single-use GMP-grade cassettes adhere to regulatory guidelines for clinical use and obviate cleaning and drying of the module between consecutive batches [35]. Boudjemeline et al. 2017 reported the first cassette-based [11C]PiB production and excluded preparative-HPLC; the same Sep Pak C18 cartridge performed purification and formulation to improve automation and routine application of [11C]PiB PET. Another dual method was the use of Synthra auto-synthesis module to convert $[^{11}C]CO_2$ to [11C]CH_3OTf. It was then then transferred to the cassette-based Scintomics GRP automated module for [11C]PiB radiolabeling and purification [35].

Our group reported a fully-automated, single module, cassette-based [11C]PiB synthesis procedure for both [11C]MeOTf preparation and [11C]PiB radiolabeling on the Trasis AllinOne with MA acceptable for clinical application [36].

Recently a GE FastLab kit method was reported that could handle two consecutive [11C]PiB productions on the same cassette, thus increasing the number of productions, with no burden on the infrastructure. This method required separate production(s) of [11C]MeOTf on GE TracerLab FXc Pro, which was transferred to the kit for further production steps. From **Table 1**, this method also had the highest reported MA [26].

Steps to improve [11C]PiB radiolabeling yields and specific activity: Significantly higher radiochemical yields (44 ± 10%) were reported when [11C]MeOTf, rather than [11C]MeI, was used as ^{11}C-methylation agent [46]. Anhydrous Na_2SO_4 or 4 Å molecular sieves can be applied as drying agents to improve yields of the water sensitive [11C]MeOTf radiolabeling reaction [47]. $MgSO_4$ has also been reported as a desiccant for the cyclohexanone solvent used during the methylation step [30].

Preparation and dilution of the reagents inside an inert atmosphere glove bag (or box) ensures high specific activ-

Table 1. Summary of radiolabeling conditions of reported [^{11}C]PiB synthesis

Precursor	^{11}C-synthon generation	Radiolabeling conditions	Radiolabeling temperature (°C)	Radiolabeling time (min)	Yield (%)	MA** (GBq/μmol)	Reference (chronological)
6-MOMO-BTA-0 (1.5 mg)	[^{11}C]CO_2→[^{11}C]MeI (Wet method)	DMSO (0.4 mL) + 10 mg KOH	125	5 + 5 (deprotection)	28.2 (of synthon)	210	[16]
6-OH-BTA-0 (0.4 mg)	[^{11}C]CO_2→[^{11}C]MeOTf (Wet method)	Loop reaction; MEK (0.08 mL)	20	1	11-16 (of [^{11}C]CO_2)	30-60	[28]
6-OH-BTA-0 (4-8 mg)	[^{11}C]CO_2→[^{11}C]MeOTf (Gas method)	Acetone (0.5 mL) cooled to -20°C during bubbling	80	1	44 ± 10 (of synthon)	80-120	[46]
6-OH-BTA-0 (1 mg)	[^{11}C]CO_2→[^{11}C]MeOTf (Wet method)	Loop reaction; Cyclohexanone (0.08 mL)	RT*	1	13-15 (of [^{11}C]CO_2)	20-60	[30]
6-OH-BTA-0 (1 mg)	[^{11}C]CO_2→[^{11}C]MeOTf (Wet method)	MEK (200 μL), with bubbling	80	1	18 (of [^{11}C]CO_2 decay corrected)	9.25	[45]
6-OH-BTA-0 (1 mg)	[^{11}C]CH_4→[^{11}C]MeOTf (Gas method)	Loop reaction; acetone/acetonitrile (0.1 mL 1:1 mixture)	RT*	1	32.9 (from [^{11}C]MeI decay corrected)	143 ± 26	[24]
6-OH-BTA-0 (2 mg)	[^{11}C]CO_2→[^{11}C]MeOTf (Gas method)	0.5 mL MEK (cooled to 13°C during bubbling)	75	2	48 (of synthon decay corrected)	183 ± 14	[21]
6-OH-BTA-0 (1 mg)	[^{11}C]CO_2→[^{11}C]MeOTf (Gas method)	Loop reaction; 3-pentanone (0.1 mL)	RT*	5	1.6 (of [^{11}C]CO_2)	265.5	[44]
6-OH-BTA-0 (1 mg)	[^{11}C]CO_2→[^{11}C]MeOTf (Wet method)	Loop reaction; acetone/acetonitrile (0.1 mL 1:1 mixture)	RT*	1	Not reported	25 ± 10	[31]
6-OH-BTA-0 (1.7 mg)	[^{11}C]CO_2	0.4 mL Diglyme + $ZnCl_2$ (1.3 mg) + IPr (3.5 mg) + $PhSiH_3$ (23 μL) cooled to 0°C during bubbling	150	20	38 (of [^{11}C]CO_2)	15	[19]
6-OH-BTA-0 (0.5-1 mg)	[^{11}C]CO_2→[^{11}C]MeOTf (Gas method)	0.3-0.5 mL MEK (cooled to 13°C during bubbling)	75	2	35-50 (of synthon decay corrected)	44.4-107.3	[27]
6-OH-BTA-0 (0.1-0.3 mg)	[^{11}C]CO_2→[^{11}C]MeOTf (Gas method)	C18 Solid phase supported radiosynthesis: acetone (50-150 μL)	RT*	2-3	22 (of synthon)	190	[35]
6-OH-BTA-0 (0.6-0.9 mg)	[^{11}C]CO_2→[^{11}C]MeOTf (Gas method)	Acetone (cooled to -40°C during bubbling, 3 min)	110	2	Not reported	≥ 7.07 specification, MA not reported	[7]
6-OH-BTA-0 (1.2-4.8 mg)	[^{11}C]CO_2	Diglyme (0.5 mL) + $PhSiH_3$ (37 μL)/TBAF 1.0 M (10 μL)	150	1	14.8 ± 12.1 (of [^{11}C]CO_2 decay corrected)	61.4 ± 1.6	[17]
6-OH-BTA-0 (1 mg)	[^{11}C]CO_2→[^{11}C]MeOTf (Wet method)	C18 Solid phase supported radiosynthesis: acetone (500 μL)	65	1	9.8 ± 1.7 (of [^{11}C]CO_2)	57 ± 18	[36]
6-OH-BTA-0 (0.3 mg)	[^{11}C]CO_2→[^{11}C]MeOTf (Gas method)	C18 Solid phase supported radiosynthesis: MEK (150 μL)	RT*	1.5	10.13 (calculated from synthon activity reported)	824.8 ± 177	[26]

*RT, Room temperature. **MA, molecular activity - converted to GBq/μmol if reported in another unit.

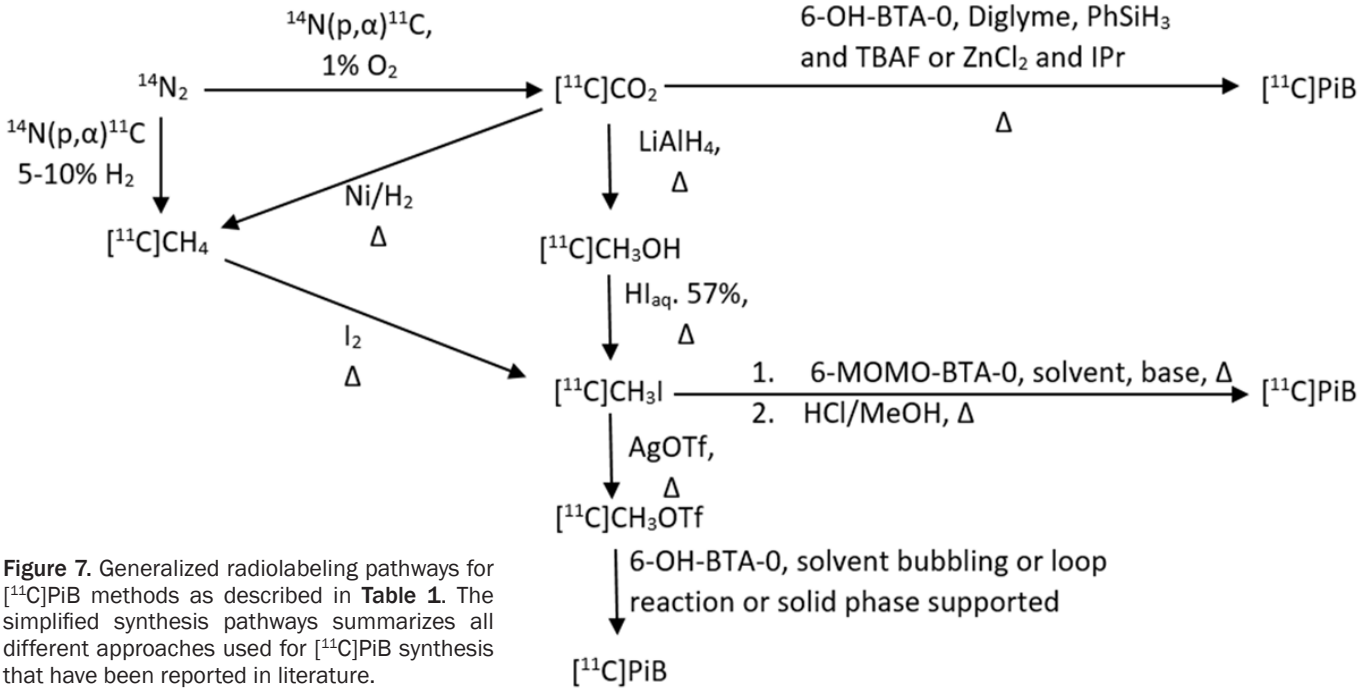

Figure 7. Generalized radiolabeling pathways for [^{11}C]PiB methods as described in **Table 1**. The simplified synthesis pathways summarizes all different approaches used for [^{11}C]PiB synthesis that have been reported in literature.

ity of the final [^{11}C]PiB product, specifically when $LiAlH_4$ is used in the synthesis [45].

To further enhance anhydrous conditions, the reactor can be rinsed with acetone, flushed with helium and dried under vacuum at 100°C for 30 min. The reactor was then cooled to 25°C and kept under a positive pressure and ultra-pure helium, before delivering radioactivity to the auto synthesis module, to perform the radiochemistry [17]. Blow drying the auto synthesis unit's lines with nitrogen gas (1 bar) for 1 hour prior to radiolabeling has also been reported to increase yields [30].

Bubbling ^{11}C-methylation reaction: The first methodology used in [^{11}C]PiB radiolabeling was bubbling ^{11}C-methylation [16] and it is still being used [35]. Some reported examples of the reaction mixture being cooled (13°C MEK and -20°C acetone) prior to transfer and improve the capture of [^{11}C]MeOTf during the bubbling process [21, 46].

Loop ^{11}C-methylation reaction: The loop reaction, or captive solvent method has been reported for both [^{11}C]MeOTf and [^{11}C]MeI radiotracer methylation reactions [47] including PiB radiolabeling [28]. Briefly, the normethyl precursor (0.4 mg), dissolved in 80 µL dimethyl formamide (DMF) or DMSO or MEK with base added (for [^{11}C]MeI) and the crude reaction mixture was loaded onto a semi-preparative HPLC injection loop (2 mL) set to the load position. The [^{11}C]MeOTf or [^{11}C]MeI was then passed through the coated HPLC loop with a stream of N_2 gas at room temperature. A proximal γ detector monitors radioactivity captured, after a peak was observed, N_2 flow ceases; the loop position was switched to inject position, and the contents are transferred onto the HPLC purification column [28, 44, 47, 48].

Solid phase supported ^{11}C-methylation reaction: Sorbent-supported radiolabeling is well-established and has been used to produce several ^{11}C-tracers [49] including [^{11}C]PiB [26, 35, 36]. The process involves passing ~100 µL of 6-OH-BTA-0 (~2 mg/mLin acetone) over a disposable Sep-Pak C18 cartridge under a stream of N_2 or Ar, effectively drying the acetone and leaving only the precursor. The radiolabeling method involves passing gaseous [^{11}C]MeOTf through the preloaded Sep-Pak C18 cartridge. Once a proximal radiodetector determines that the maximal amount of [^{11}C]MeOTf was trapped on the Sep-Pak cartridge, it was allowed to react with the precursor for 2 minutes at room temperature or heating to 65°C [35, 36]. The final [^{11}C]PiB was then eluted for further purification and/or formulation.

Preparative HPLC and purification methods for [^{11}C]PiB

Considering pKa values of PiB are essential to ensure sharp peak shapes in HPLC and trapping on SPE cartridges, the phenol had a pKa value of 9.3, and methylamine (protonated) group was 3.0 [16]. **Table 2** summarizes all reported prep-HPLC or other purification technique parameters.

Reformulation

According to USP 823, facilities, equipment, and procedures must ensure a sterile PET product, although its sterility can only be tested through incubated growth after use. The chemical synthesis of a parenterally administered radiotracer may take place in an open or closed sys-

Table 2. Preparative HPLC or other purification technique conditions

Mobile phase	pH	Phase (Column)	Flow rate (ml/min)	Reported retention time (min)	Reference (chronological)
35% Acetonitrile/65% triethylammonium phosphate buffer	7.2	C18 (Phenomenex Prodigy 10 µm ODS-prep 10 × 250 mm)	15	11.5	[16]
40% Acetonitrile/60% aqueous 0.1 N NH_4HCO_2	Not reported	C18 (Phenomenex Luna 10 µm, 10 × 250 mm)	9	9	[28]
75% Acetonitrile/25% aqueous 0.2% triethylammonium acetate	7.3	C18 (Supelco ABZ+ 5 µm, 250 × 10 mm)	8	4.5	[46]
50% Acetonitrile/50% water	Not reported (± 7)	C18 (Waters, 7 µm, 7.8 × 300 mm)	3	7	[30]
40% Acetonitrile/60% aqueous 0.1 N ammonium formate	Not reported	C18 (Alltech Alltima 5 µm; 250 mm × 10 mm)	7	10-11	[45]
60% Acetonitrile/40% aqueous 0.01 M sodium acetate	9	C18 (Macherey-Nagel Nucleosil 100-7 C18, 250 × 16 mm)	8	8-9	[24]
60% Acetonitrile/40% aqueous 0.1 M ammonium acetate/0.2% 2 M triethylammonium acetate	Not reported	C18 (Supelcosil LC-ABZ+ 5 µm, 250 mm × 10 mm)	8	4.9	[21]
40% Acetonitrile/60% aqueous 50 mM ammonium acetate	Not reported	C18 (Phenomonex Luna C18, 150 × 10 mm)	5	~8	[44]
40% Acetonitrile/60% aqueous 0.1 N ammonium formate	Not reported	C18 (Phenomenex Luna 5 µm, 10 × 250 mm)	9	7-8	[31]
40% Acetonitrile/60% water	Not reported (± 7)	C18 (Waters Symmetry-Prep 7 µm, 7.8 × 300 mm)	4	11	[19]
40% Ethanol/60% 0.01 M trisodiumcitrate; 0.1% ascorbic acid	Not reported (acidic)	C18 (Phenomenex Luna 10 µm, 10 × 250 mm)	6	13-16	[27] Method A
40% Acetonitrile/60% 0.01 M-trisodiumcitrate; 0.1% ascorbic acid	3.5	C18 (Agilent Eclipse XDB 5 µm ODS-prep 9.4 × 250 mm)	4.5	9-11	[27] Method B
2.5 mL of 50% EtOH/acetate buffer	3.7	*C18 SPE purification was achieved through selective washing and elution*			[35]
50% Acetonitrile/50% water	Not reported (± 7)	C18 (Phenomenex Luna 5 µm 100 Å 250 × 10 mm)	4	8.5-9.5	[17]
60% Acetonitrile/40% water	Not reported (± 7)	C18 (Waters XBridge BEH Shield RP18 OBD, 130 Å, 5 µm, 10 × 250 mm)	5	4.5	[36]
2.5 mL of 50% EtOH/acetate buffer	3.7	*C18 SPE purification was achieved through selective washing and elution*			[26]

tem, so some steps can be performed on a bench top. However, all activities downstream of the 0.22 μm membrane filter should be conducted in a closed, sterile system to minimize contamination risk. Radiopharmaceuticals must be dispensed in a clean room, hot cell, biosafety cabinet, or other environment with an ISO 5 or lower rating [50].

Reformulation steps for [11C]PiB were very standardized, with little-to-no variation reported in the literature. The fraction collected from the preparative HPLC was diluted with water (20-100 mL), trapped on a C18 SPE cartridge, optionally washed with water (0-15 mL), eluted with ethanol (1 mL), and then diluted with physiologic solution or saline to reduce the ethanol concentration to ≤ 10%. The final product was then filtered through a 0.22 μm membrane filter into the final product vial [21, 24, 46]. Some groups add 1 mL of phosphate buffer (125 mM) [21] or another fraction of saline [36] to the final product. In an exception to the standardized reformulation method, radiolabeling was carried out and the reaction mixture purified and formulated on the same C18 SPE cartridge, using a 50% ethanol solution as eluent [26, 35].

Total synthesis time comparison

For routine preparation and high resolution [11C]PiB PET images, the total synthesis time is important; the longer the radio decay period, the lower the MA expressed as GBq/μg [25]. For saturable processes (e.g., receptors on proteins) competition between the [11C]PiB and indistinguishable cold PiB impairs the quality of the PET scan data. Therefore, MA has been identified as a key factor in both preclinical and clinical studies dealing with tracer-binding densities [23].

Total synthesis time for recent automated procedures ranges from 20 to 35 minutes as measured after the end of bombardment. For examples of total synthesis time was ~25 min [36]; 32 min [17]; 20 min [35]; 30 min [27]; 25-30 min [31]; 35 min [26]. The fastest reported synthesis method of 20 min, did not include preparative HPLC, indicating the efficiency of optimized SPE purification and formulation methods [35]. The slowest method had reported the highest MA [26].

We believe that most of the radiolabeling strategies (**Table 1**) can be used with any of the purification methods (**Table 2**), which might lower the total synthesis time significantly. A laboratory considering implementing a new synthesis strategy for [11C]PiB or optimizing their existing production method, can identify a radiolabeling and purification method that best suits their facility needs.

Quality control (QC) considerations

Every batch of [11C]PiB intended for human use must undergo around 9 QC tests before it can be administered. They include: 1) visual inspection and assess, 2) pH, 3) radiochemical purity, 4) radionuclide identity, 5) PiB identity and concentration, 6) molar activity, 7) residual solvent analysis, 8) chemical purity, and 9) stabilizer concentration (if any) [50]. Every production facility must meet parameters and document specifications for each [11C]PiB synthesis procedure prior to administering a batch [18].

Optimizing the HPLC-UV method can significantly improve MA and activity concentrations at the time of injection [23]. The HPLC-UV chromatogram should show clear separation of the solvent front, precursor and PiB peaks at baseline level [22]. Several strategies can reduce HPLC-UV QC run time; for example, by increasing the flow rate and temperature, while reducing the particle size and column volume using a thinner or shorter column. A compliant [11C]PiB HPLC-UV can be run in as little as two minutes [23]. The literature reports an upper limit of 13.4 μg of PiB per injection and with a lower limit of 1.34 μg of 6-OH-BTA-0 per injection [7, 26]. We have recently published a review on the QC design process for 11C-tracers which highlights all the aspects of each of nine QC tests [51].

Releasing a [11C]PiB batch for a clinical PET scan

After the appropriate QC tests are completed and the data and documentation have been reviewed [52], a designated qualified expert authorizes the use of the [11C]PiB final batch by dated signature. Certain QC tests, such as sterility tests can be performed as post-release controls, provided the synthesis procedure has been well validated [7, 50]. A conditional release or reprocessing may be possible if one of the QC tests could not be completed or obtained a questionable result but only under certain conditions and with written procedures in place [50, 52].

Overview of [11C]PiB PET imaging applications

[11C]PiB is the most commonly used Aβ plaque imaging radiotracer due to its fast uptake and low nonspecific binding in the human brain [17, 27]. Many clinical studies support its effectiveness in correlating of Aβ plaques with Alzheimer's disease (AD) progression and mild cognitive impairment (MCI) [53]. Zhang et al., reported a systematic review on the use of [11C]PiB PET for the early diagnosis of AD and an assessment of the effectiveness and accuracy of early diagnosis. The same group also concluded that a standardized threshold for a positive result was required before [11C]PiB PET could be widely applied to clinical practice [54]. A few studies reported a comparison between [11C]PiB PET retention longitudinal assessment of Aβ deposition of healthy older adults with those of AD patients [55, 56]. [11C]PiB PET imaging can distinguish AD from frontotemporal dementia [57] and frontotemporal lobar degeneration [58]. Aging effect of Aβ deposition in non-demented adults with down syndrome has been studied using [11C]PiB PET, indicating an age-related

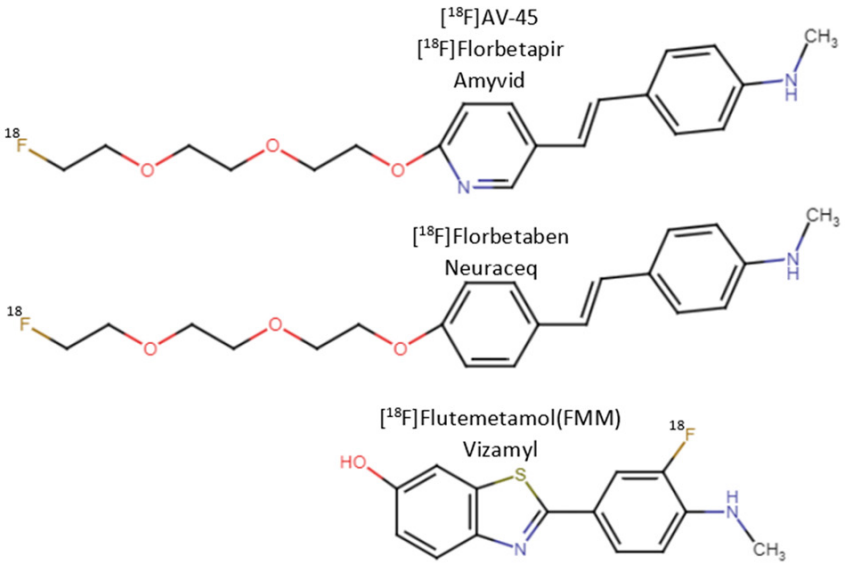

Figure 8. Aβ-plaque PET imaging agents approved by the US Food and Drug Administration. The chemical structure of all the FDA approved Aβ-plaque PET imaging agents, for visual comparison with the [11C]PiB structure.

deposition Aβ plaques in the down Syndrome population [59].

A proposed amyloid quantification index (AQI) can reportedly differentiate MCI from AD in otherwise clinically indistinguishable AD cases. A 30-min [11C]PiB PET scan can estimated AQI based on clearance rate and mid-phase PiB retention in featured brain regions [60].

Comparison to other radiotracers

Studies have compared the accuracy, specificity, and selectivity of [18F]FDG versus [11C]PiB for diagnosing or predicting AD. A review and statistical analysis found that PiB was more sensitive in predicting MCI progression to AD, but might have less specificity [53]. Later studies suggest a benefit in combining and interpreting the imaging data from [18F]FDG and [11C]PiB PET scans [61]. [11C]PiB PET's ability to identify AD and to distinguishing it from MCI has also been compared to [18F]FDDNP. It was reported that for the identification of AD and differences in non-displaceable binding potential between patients with AD, patients with MCI, and controls were more pronounced using [11C]PiB PET. Difference in regional binding were moderately correlated suggesting that the two radiotracers adsorb to related, but different characteristic brain regions of AD [62].

The FDA approved [18F]flutemetamol (FMM) radiotracer is structurally related to [11C]PiB (refer to **Figure 8**). A strong correlation in standardized uptake value ratio (SUVR) was reported comparing [11C]PiB with previously scanned [18F]FMM subjects, however the SUVR for [18F]FMM PET in the AD group was lower [63]. Another similar study reported when a standardized visual read technique was applied to classify scans as Aβ-positive or Aβ-negative [18F]FFM was reported to have higher white-matter retention, and care must be taken not to interpret it as a false-positive result [64]. White matter is highly lipidic with the tissue mainly composed of myelin [65] and because [18F]FMM is more lipophilic than [11C]PiB, it has been suggested non-specific uptake might be a key factor for the increased uptake, rather than actual/specific target protein uptake [66]. This was also studied for [11C]PiB both *in vitro* and *in vivo* [67] conditions. Studying uptake of [11C]PiB in white matter has been proven to be useful in identifying lesions and studying multiple sclerosis [68] non-specific for AD. Targeted binding of [18F]FMM to Aβ protein was also characterized as a slow kinetic component [66].

Although [18F]Florbetaben is not structurally related to [11C]PiB (**Figure 8**), it exhibits a high affinity for Aβ-plaques and can distinguish between AD positive and negative patients. However, [18F]Florbetaben has been reported to have a lower degree of retention, for a narrower dynamic range of SUVR values than [11C]PiB. This was demonstrated through total SUVR for [11C]PiB in AD patients that was 75% greater than in healthy subjects while only 56% greater for [18F]Florbetaben [69].

Further, [18F]florbetapir or [18F]AV-45, was found to have similar binding characteristics compared to [11C]PiB, with [18F]AV-45 PET able to discriminate healthy controls from mild AD. However, the SUVR contrast between the lowest and highest uptake regions was higher for [11C]PiB PET scans. It was theorized this may be due to higher non-specific white matter uptake of [18F]AV-45 [70]. A more recent study, by Chen et al., 2023, into anti-amyloid-β monoclonal antibodies effects were found statistically significant across both [11C]PiB and [18F]AV-45 radiotracers. For one of the treatments, gantenerumab, [11C]PiB SUVRs decreased more rapidly than that of [18F]AV-45. Type 1 error is reduced in clinical trials that only used one Aβ-tracer to evaluate Aβ treatment effects, and overall power was lower in trails using [18F]AV-45 compared to [11C]PiB [71]. [18F]AV-45 has been described as lipophilic [72], thus in a similar manner to [18F]FMM, has been theorized to have non-specific uptake into white matter [73]. There is no observable difference between [11C]PiB and [18F]AV-45 white matter uptake [67, 74]. However, studying [18F]AV-45 uptake in white matter reveals a slight difference in AD patients and healthy individuals. The difference is too subtle for using the SUVR approach and MANOVA and discriminant analyses is required to observe it. Nevertheless, this information could reveal white matter modifications [65].

Limitations of [^{11}C]PiB

Some limitations have been identified in [^{11}C]PiB PET-based diagnosis of AD. Aβ plaques have diverse structures; many include massed, fibrillar polymers, but some lack the defining features of amyloids. In particular, [^{11}C]PiB affinity for cotton wool plaques, common in familial AD but rare in sporadic AD was problematic [75, 76]. A mutation of the PSEN1 gene associated with familial AD produces a high cortical fibrillar Aβ load and lower than expected cortical [^{11}C]PiB retention in the brain [75].

Further, Aβ deposits have been reported in approximately a third of asymptomatic older adults. *In vivo* Aβ imaging comparing functional magnetic resonance imaging (fMRI) activity with [^{11}C]PiB PET imaging of the cortical regions, collectively known as the default network, demonstrates that high levels of Aβ deposition can be correlated with the observed fMRI activity in asymptomatic, dementia-free older individuals. Whether they will develop clinical dementia or AD [77] remains unknown.

Some evidence indicates that Aβ plaque deposits are necessary but not sufficient to cause the cognitive dysfunction associated with AD [78]. Fibrillar Aβ detected by [^{11}C]PiB PET can increase over time in older adults without causing dementia; further research is required to identify factors that explain this resilience to Aβ deposition [55, 56]. A longitudinal assessment of Aβ deposition increase and cognition decline was found to be weakly correlated, suggesting that downstream factors affect the progression of AD and MCI symptoms [56]. Although β-amyloid deposition precedes AD and MCI, β-amyloid levels may not strongly correlate with cognitive impairment of AD patients [79] and MCI appears to be brought about by other factors or a combination of factors [39]. A recent study suggests a correlation of vascular risk factors and AD processes leading to MCI [80].

Similar to [^{11}C]PiB, [^{18}F]AV-45 has high affinity for Aβ-plaques; however, because of longer half-life of fluorine-18 (^{18}F), uptake time can be extended, and a stable plateau accumulates within 50 minutes allowing robust imaging and easier application of more than one dose per batch [81].

Views of authoritative and legislative bodies on PET radiopharmaceuticals

The National Institute on Aging-Alzheimer's Association (NIA-AA) criteria for AD neuropathological diagnosis was revised a decade ago to include all Aβ-immunoreactive plaques, assessed according by phases of its deposition [82, 83]. In 2014, The U.S. Food and Drug Administration (FDA) adjudged that licensed amyloid ligand tests do not establish a positive diagnosis of AD nor predict progression from MCI to AD [54]. The current view of the field seems to hold that although AD pathogenesis remains unclear, there are several mechanisms to be considered including Aβ protein deposition, tau protein hyperphosphorylation, inflammation, oxidative stress, mitochondrial, and cerebrovascular changes [84]. [^{11}C]PiB PET data must be combined with other neuropsychological testing to better define AD progression [85].

Although [^{11}C]PiB PET is now the gold standard for imaging Aβ plaques in the brain [17, 21], [^{18}F]AV-45 or [^{18}F]Florbetapir, registered under the trade name of Amyvid, was the first Aβ-plaque PET imaging agent approved by the US FDA in 2012 [2, 78]. Two other FDA-approved radiopharmaceuticals, Neuraceq ([^{18}F]Florbetaben) and Vizamyl ([^{18}F]Flutemetamol) were also used to estimate Aβ plaque density in the brain (**Figure 8**) (https://www.accessdata.fda.gov/scripts/cder/daf/).

Conclusion

Aβ-plaque imaging is likely to play a critical role in the development of treatments for AD by monitoring the response to anti-amyloidal therapies or other treatments and improving early treatment possibilities.

Comparing certain aspects of radiochemistry methods can be challenging. For example, yields can be reported as a percentage of a [^{11}C]synthon or the [^{11}C]CO_2 produced as corrected or uncorrected yields. A few publications do not report a % yield at all but just the total activity or specific activity obtained at the end of synthesis. Standardizing how radiochemical yield is reported would facilitate direct comparison of synthesis methods but for now, the task is daunting. MA was reported consistently for the most part in GBq/μmol. However, it varies so much even between very similar synthesis methods, we have to wonder whether the radiosynthesis method affects MA at all.

Although [^{11}C]PiB cannot be commercially shipped as the structurally similar [^{18}F]FMM or other Aβ-plaque tracers such as [^{18}F]AV-45 or [^{18}F]Florbetaben, there are still advantages of using [^{11}C]PiB in facilities that have ^{11}C radiochemistry capabilities. These advantages include lower white-matter uptake in Aβ-negative subjects, a higher dynamic rage and higher SUVR for AD positive subjects [63, 64, 69, 70].

In terms of future developments for [^{11}C]PiB synthesis, no one synthetic method combining all three optimizations reported in the literature has been reported (**Figure 1**). Hypothetically, the ideal method would use [^{11}C]CO_2 fixation [19] and have no deprotection [28] or prep-HPLC steps [35], thus minimizing potential failure points and maximizing speed. In addition, no cassette-based [^{11}C]CO_2 fixation for [^{11}C]PiB synthesis has been reported and might be worth exploring to further simplify cassette-kits.

Acknowledgements

The authors thank the staff of the Translational Imaging Program and the Department of Radiology at Atrium

Health Wake Forest Baptist Medical Center for their expertise. This work was supported by R01AG065839 (KKSS), R56AG081860 (KKSS), and P30AG072947.

Disclosure of conflict of interest

None.

Abbreviations

Aβ, amyloid-β; AD, Alzheimer's disease; AQI, Quantification index; BET, Bacterial Endotoxin Test; DMF, Dimethylformamide; DMSO, Dimethylsulfoxide; FDA, U.S. Food and Drug Administration; FMM, Flutemetamol; fMRI, functional Magnetic Resonance Imaging; GC, Gas Chromatography; HPLC, High-performance liquid chromatography; MCI, Mild cognitive impairment; MeI, Methyl Iodide - CH_3I; MEK, Methyl ethyl ketone/Butan-2-one; MeOTf, Methyl trifoliate/trifluoromethanesulfonate - $CH_3OSO_2CF_3$; PET, Positron Emission Tomography; PiB, Pittsburgh compound B/[^{11}C]6-OH-BTA-1/2-(4-N-methylaminophenyl)-6-hydroxybenzothiazole; QC, Quality Control; RT, Room temperature; SPE, Solid phase extraction; SUVR, Standardized uptake value ratio; UV, Ultra Violate.

Address correspondence to: Dr. Kiran Kumar Solingapuram Sai, Department of Radiology, Wake Forest School of Medicine, Winston-Salem, NC 27157, USA. ORCID: 0000-0002-6442-5169; E-mail: ksolinga@wakehealth.edu

References

[1] Mirra SS, Heyman A, McKeel D, Sumi SM, Crain BJ, Brownlee LM, Vogel FS, Hughes JP, van Belle G and Berg L. The Consortium to Establish a Registry for Alzheimer's Disease (CERAD). Part II. Standardization of the neuropathologic assessment of Alzheimer's disease. Neurology 1991; 41: 479-486.

[2] Holland JP, Liang SH, Rotstein BH, Collier TL, Stephenson NA, Greguric I and Vasdev N. Alternative approaches for PET radiotracer development in Alzheimer's disease: imaging beyond plaque. J Labelled Comp Radiopharm 2014; 57: 323-331.

[3] Tiraboschi P, Hansen LA, Thal LJ and Corey-Bloom J. The importance of neuritic plaques and tangles to the development and evolution of AD. Neurology 2004; 62: 1984-1989.

[4] Walker LC. Aβ plaques. Free Neuropathol 2020; 1: 1-31.

[5] Yang Y, Arseni D, Zhang W, Huang M, Lövestam S, Schweighauser M, Kotecha A, Murzin AG, Peak-Chew SY, Macdonald J, Lavenir I, Garringer HJ, Gelpi E, Newell KL, Kovacs GG, Vidal R, Ghetti B, Ryskeldi-Falcon B, Scheres SHW and Goedert M. Cryo-EM structures of amyloid-β 42 filaments from human brains. Science 2022; 375: 167-172.

[6] Yamazaki T, Yamaguchi H, Okamoto K and Hirai S. Ultrastructural localization of argyrophilic substances in diffuse plaques of Alzheimer-type dementia demonstrated by methenamine silver staining. Acta Neuropathol 1991; 81: 540-545.

[7] Bateman RJ, Xiong C, Benzinger TL, Fagan AM, Goate A, Fox NC, Marcus DS, Cairns NJ, Xie X, Blazey TM, Holtzman DM, Santacruz A, Buckles V, Oliver A, Moulder K, Aisen PS, Ghetti B, Klunk WE, McDade E, Martins RN, Masters CL, Mayeux R, Ringman JM, Rossor MN, Schofield PR, Sperling RA, Salloway S and Morris JC; Dominantly Inherited Alzheimer Network. Clinical and biomarker changes in dominantly inherited Alzheimer's disease. N Engl J Med 2012; 367: 795-804.

[8] Klunk WE. Amyloid imaging as a biomarker for cerebral beta-amyloidosis and risk prediction for Alzheimer dementia. Neurobiol Aging 2011; 32 Suppl 1: S20-36.

[9] Chetelat G, La Joie R, Villain N, Perrotin A, de La Sayette V, Eustache F and Vandenberghe R. Amyloid imaging in cognitively normal individuals, at-risk populations and preclinical Alzheimer's disease. Neuroimage Clin 2013; 2: 356-365.

[10] Pike KE, Savage G, Villemagne VL, Ng S, Moss SA, Maruff P, Mathis CA, Klunk WE, Masters CL and Rowe CC. Beta-amyloid imaging and memory in non-demented individuals: evidence for preclinical Alzheimer's disease. Brain 2007; 130: 2837-2844.

[11] Kemppainen NM, Aalto S, Wilson IA, Nagren K, Helin S, Bruck A, Oikonen V, Kailajarvi M, Scheinin M, Viitanen M, Parkkola R and Rinne JO. PET amyloid ligand [11C]PIB uptake is increased in mild cognitive impairment. Neurology 2007; 68: 1603-1606.

[12] Rowe CC, Ellis KA, Rimajova M, Bourgeat P, Pike KE, Jones G, Fripp J, Tochon-Danguy H, Morandeau L, O'Keefe G, Price R, Raniga P, Robins P, Acosta O, Lenzo N, Szoeke C, Salvado O, Head R, Martins R, Masters CL, Ames D and Villemagne VL. Amyloid imaging results from the Australian Imaging, Biomarkers and Lifestyle (AIBL) study of aging. Neurobiol Aging 2010; 31: 1275-1283.

[13] El-Gamal FEZA, Elmogy MM, Ghazal M, Atwan A, Barnes GN, Casanova MF, Keynton R and El-Baz AS. A novel CAD system for local and global early diagnosis of Alzheimer's disease based on PIB-PET scans. 2017 IEEE international conference on image processing (ICIP). IEEE 2017; 3270-3274.

[14] Cohen AD, Rabinovici GD, Mathis CA, Jagust WJ, Klunk WE and Ikonomovic MD. Using Pittsburgh Compound B for in vivo PET imaging of fibrillar amyloid-beta. Adv Pharmacol 2012; 64: 27-81.

[15] Klunk WE, Engler H, Nordberg A, Wang Y, Blomqvist G, Holt DP, Bergstrom M, Savitcheva I, Huang GF, Estrada S, Ausen B, Debnath ML, Barletta J, Price JC, Sandell J, Lopresti BJ, Wall A, Koivisto P, Antoni G, Mathis CA and Langstrom B. Imaging brain amyloid in Alzheimer's disease with Pittsburgh Compound-B. Ann Neurol 2004; 55: 306-319.

[16] Mathis CA, Wang Y, Holt DP, Huang GF, Debnath ML and Klunk WE. Synthesis and evaluation of 11C-labeled 6-substituted 2-arylbenzothiazoles as amyloid imaging agents. J Med Chem 2003; 46: 2740-2754.

[17] Buccino P, Savio E and Porcal W. Fully-automated radiosynthesis of the amyloid tracer [(11)C] PiB via direct [(11)C]CO(2) fixation-reduction. EJNMMI Radiopharm Chem 2019; 4: 14.

[18] Damuka N and Solingapuram Sai KK. Method to development of PET radiopharmaceutical for cancer imaging. Methods Mol Biol 2022; 2413: 13-22.

[19] Liger F, Eijsbouts T, Cadarossanesaib F, Tourvieille C, Le Bars D and Billard T. Direct [11C]methylation of amines from [11C]CO_2 for the synthesis of PET radiotracers. European J Org Chem 2015; 2015: 6434-6438.

[20] Antoni G. Development of carbon-11 labelled PET tracers-radiochemical and technological challenges in a historic perspective. J Labelled Comp Radiopharm 2015; 58: 65-72.
[21] Philippe C, Haeusler D, Mitterhauser M, Ungersboeck J, Viernstein H, Dudczak R and Wadsak W. Optimization of the radiosynthesis of the Alzheimer tracer 2-(4-N-[11C] methylaminophenyl)-6-hydroxybenzothiazole ([11C]PIB). Appl Radiat Isot 2011; 69: 1212-1217.
[22] Passchier J. Fast high performance liquid chromatography in PET quality control and metabolite analysis. Q J Nucl Med Mol Imaging 2009; 53: 411-6.
[23] Nics L, Steiner B, Klebermass EM, Philippe C, Mitterhauser M, Hacker M and Wadsak W. Speed matters to raise molar radioactivity: fast HPLC shortens the quality control of C-11 PET-tracers. Nucl Med Biol 2018; 57: 28-33.
[24] Gomez-Vallejo V and Llop J. Fully automated and reproducible radiosynthesis of high specific activity [(1)(1)C]raclopride and [(1)(1)C]Pittsburgh compound-B using the combination of two commercial synthesizers. Nucl Med Commun 2011; 32: 1011-1017.
[25] Luurtsema G, Pichler V, Bongarzone S, Seimbille Y, Elsinga P, Gee A and Vercouillie J. EANM guideline for harmonisation on molar activity or specific activity of radiopharmaceuticals: impact on safety and imaging quality. EJNMMI Radiopharm Chem 2021; 6: 34.
[26] Nair M, Cheung YY, Liu F, Koran ME and Rosenberg AJ. Fully automated dual-run manufacturing of [11C]PIB on FASTlab. Nucl Med Biol 2023; 128-129: 108873.
[27] Coliva A, Monterisi C, Apollaro A, Gatti D, Penso M, Gianolli L, Perani D, Gilardi MC and Carpinelli A. Synthesis optimization of 2-(4-N-[11C]methylaminophenyl)-6-hydroxybenzothiazole ([11C]PIB), beta-amyloid PET imaging tracer for Alzheimer's disease diagnosis. Appl Radiat Isot 2015; 105: 66-71.
[28] Wilson AA, Garcia A, Chestakova A, Kung H and Houle S. A rapid one-step radiosynthesis of the β-amyloid imaging radiotracer N-methyl-[11C]2-(4'-methylaminophenyl)-6-hydroxybenzothiazole([11C]-6-OH-BTA-1). J Labelled Comp Radiopharm 2004; 47: 679-682.
[29] Joshi RK, Goud NS, Nagaraj C, Kumar D, R G, Rao NP, Dhawan A, Bhattacharya A, Mangalore S, Bharath RD and Kumar P. Radiosynthesis challenges of (11)C and (18)F-labeled radiotracers in the FX2C/N tracerlab and their validation through PET-MR imaging. Appl Radiat Isot 2021; 168: 109486.
[30] Verdurand M, Bort G, Tadino V, Bonnefoi F, Le Bars D and Zimmer L. Automated radiosynthesis of the Pittsburg compound-B using a commercial synthesizer. Nucl Med Commun 2008; 29: 920-926.
[31] Clemente G, Alves V and Abrunhosa AJ. Synthesis optimization of pittsburgh compound B by the captive solvent method. 2012 IEEE 2nd Portuguese Meeting in Bioengineering (ENBENG). IEEE 2012; 1-4.
[32] Larsen P, Ulin J, Dahlstrøm K and Jensen M. Synthesis of [11C]iodomethane by iodination of [11C]methane. Appl Radiat Isot 1997; 48: 153-157.
[33] Crouzel C, Langstrom B, Pike VW and Coenen HH. Recommendations for a practical production of [C-11] methyl-Iodide. Appl Radiat Isot 1987; 38: 601-603.
[34] Fowler J and Wolf A. Synthesis of carbon-11, fluorine-18, and nitrogen-13 labeled radiotracers for biomedical applications. Nuclear Science Series: Nuclear Medicine. 1982.
[35] Boudjemeline M, Hopewell R, Rochon PL, Jolly D, Hammami I, Villeneuve S and Kostikov A. Highly efficient solid phase supported radiosynthesis of [(11) C]PiB using tC18 cartridge as a "3-in-1" production entity. J Labelled Comp Radiopharm 2017; 60: 632-638.
[36] Myburgh PJ, Moore MD, Pathirannahel BL, Grace LR and Solingapuram Sai KK. Fully automated production of [11C]PiB for clinical use on Trasis-AllinOne synthesizer module. Appl Radiat Isot 2023; 202: 111040.
[37] Zhang MR and Suzuki K. Sources of carbon which decrease the specific activity of [11C]CH3I synthesized by the single pass I2 method. Appl Radiat Isot 2005; 62: 447-450.
[38] Jewett DM. A simple synthesis of [11C]methyl triflate. Int J Rad Appl Instrum A 1992; 43: 1383-1385.
[39] Jewett EM, Nagren K, Mock BH and Watkins GL. 30 years of [(11)C]methyl triflate. Appl Radiat Isot 2023; 197: 110812.
[40] Pees A, Chasse M, Lindberg A and Vasdev N. Recent developments in carbon-11 chemistry and applications for first-in-human PET studies. Molecules 2023; 28: 931.
[41] Alder RW, Phillips JG, Huang L and Huang X. Methyltrifluoromethanesulfonate. Encyclopedia of Reagents for Organic Synthesis. 2005.
[42] Jacquet O, Das Neves Gomes C, Ephritikhine M and Cantat T. Recycling of carbon and silicon wastes: room temperature formylation of N-H bonds using carbon dioxide and polymethylhydrosiloxane. J Am Chem Soc 2012; 134: 2934-2937.
[43] Jacquet O, Frogneux X, Das Neves Gomes C and Cantat T. CO_2 as a C1-building block for the catalytic methylation of amines. Chem Sci 2013; 4: 2127-2131.
[44] Shao X, Hoareau R, Runkle AC, Tluczek LJM, Hockley BG, Henderson BD and Scott PJH. Highlighting the versatility of the Tracerlab synthesis modules. Part 2: fully automated production of [11C]-labeled radiopharmaceuticals using a Tracerlab FXC-Pro. J Labelled Comp Radiopharm 2011; 54: 819-838.
[45] Cheung MK and Ho CL. A simple, versatile, low-cost and remotely operated apparatus for [11C]acetate, [11C]choline, [11C]methionine and [11C]PIB synthesis. Appl Radiat Isot 2009; 67: 581-589.
[46] Solbach C, Uebele M, Reischl G and Machulla HJ. Efficient radiosynthesis of carbon-11 labelled uncharged Thioflavin T derivatives using [11C]methyl triflate for beta-amyloid imaging in Alzheimer's Disease with PET. Appl Radiat Isot 2005; 62: 591-595.
[47] Ono M, Wilson A, Nobrega J, Westaway D, Verhoeff P, Zhuang ZP, Kung MP and Kung HF. 11C-labeled stilbene derivatives as Abeta-aggregate-specific PET imaging agents for Alzheimer's disease. Nucl Med Biol 2003; 30: 565-571.
[48] Wilson AA, Garcia A, Jin L and Houle S. Radiotracer synthesis from [(11)C]-iodomethane: a remarkably simple captive solvent method. Nucl Med Biol 2000; 27: 529-532.
[49] Watkins GL, Jewett DM, Mulholland GK, Kilbourn MR and Toorongian SA. A captive solvent method for rapid N-[11C] methylation of secondary amides: application to the benzodiazepine, 4'-chlorodiazepam (RO5-4864). Int J Rad Appl Instrum A 1988; 39: 441-444.
[50] USP<823>. United States Pharmacopia (USP) chapter <823>Positron Emission Tomography Drugs for compounding, investigational and research uses. 2011; USP 35.

[51] Myburgh PJ and Sai KKS. Development and optimization of 11C-labeled radiotracers: a review of the modern quality control design process. ACS Pharmacol Transl Sci 2023; 6: 1616-1631.
[52] FDA_Title_21. Food and Drug Administration(FDA)-Code of Federal Regulations (CFR) - Title 21 CFR Part 212 Current Good Manufacturing Practice for Positron Emission Tomography Drugs. 21 CFR Part 212 2023.
[53] Zhang S, Han D, Tan X, Feng J, Guo Y and Ding Y. Diagnostic accuracy of 18F-FDG and 11C-PIB-PET for prediction of short-term conversion to Alzheimer's disease in subjects with mild cognitive impairment. Int J Clin Pract 2012; 66: 185-198.
[54] Zhang S, Smailagic N, Hyde C, Noel-Storr AH, Takwoingi Y, McShane R and Feng J. (11)C-PIB-PET for the early diagnosis of Alzheimer's disease dementia and other dementias in people with mild cognitive impairment (MCI). Cochrane Database Syst Rev 2014; 2014: CD010386.
[55] Sojkova J, Zhou Y, An Y, Kraut MA, Ferrucci L, Wong DF and Resnick SM. Longitudinal patterns of beta-amyloid deposition in nondemented older adults. Arch Neurol 2011; 68: 644-649.
[56] Villemagne VL, Pike KE, Chételat G, Ellis KA, Mulligan RS, Bourgeat P, Ackermann U, Jones G, Szoeke C, Salvado O, Martins R, O'Keefe G, Mathis CA, Klunk WE, Ames D, Masters CL and Rowe CC. Longitudinal assessment of Aβ and cognition in aging and Alzheimer disease. Ann Neurol 2011; 69: 181-192.
[57] Engler H, Santillo AF, Wang SX, Lindau M, Savitcheva I, Nordberg A, Lannfelt L, Langstrom B and Kilander L. In vivo amyloid imaging with PET in frontotemporal dementia. Eur J Nucl Med Mol Imaging 2008; 35: 100-106.
[58] Rabinovici GD, Furst AJ, O'Neil JP, Racine CA, Mormino EC, Baker SL, Chetty S, Patel P, Pagliaro TA, Klunk WE, Mathis CA, Rosen HJ, Miller BL and Jagust WJ. 11C-PIB PET imaging in Alzheimer disease and frontotemporal lobar degeneration. Neurology 2007; 68: 1205-1212.
[59] Lao PJ, Betthauser TJ, Hillmer AT, Price JC, Klunk WE, Mihaila I, Higgins AT, Bulova PD, Hartley SL, Hardison R, Tumuluru RV, Murali D, Mathis CA, Cohen AD, Barnhart TE, Devenny DA, Mailick MR, Johnson SC, Handen BL and Christian BT. The effects of normal aging on amyloid-beta deposition in nondemented adults with Down syndrome as imaged by carbon 11-labeled Pittsburgh compound B. Alzheimers Dement 2016; 12: 380-390.
[60] Shen C, Wang Z, Chen H, Bai Y, Li X, Liang D, Liu X, Zheng H, Wang M, Yang Y, Wang H and Sun T. Identifying mild Alzheimer's disease with first 30-min 11C-PiB PET scan. Front Aging Neurosci 2022; 14: 785495.
[61] Liu F, Shi Y, Wu Q, Chen H, Wang Y, Cai L and Zhang N. The value of FDG combined with PiB PET in the diagnosis of patients with cognitive impairment in a memory clinic. CNS Neurosci Ther 2023; 30: e14418.
[62] Tolboom N, Yaqub M, Van Der Flier WM, Boellaard R, Luurtsema G, Windhorst AD, Barkhof F, Scheltens P, Lammertsma AA and Van Berckel BN. Detection of Alzheimer pathology in vivo using both 11C-PIB and 18F-FDDNP PET. J Nucl Med 2009; 50: 191-197.
[63] Hatashita S, Wakebe D, Kikuchi Y and Ichijo A. Longitudinal assessment of amyloid-beta deposition by [18F]-flutemetamol PET imaging compared with [11C]-PIB across the spectrum of Alzheimer's disease. Front Aging Neurosci 2019; 11: 251.
[64] Mountz JM, Laymon CM, Cohen AD, Zhang Z, Price JC, Boudhar S, McDade E, Aizenstein HJ, Klunk WE and Mathis CA. Comparison of qualitative and quantitative imaging characteristics of [11C]PiB and [18F]flutemetamol in normal control and Alzheimer's subjects. Neuroimage Clin 2015; 9: 592-598.
[65] Nemmi F, Saint-Aubert L, Adel D, Salabert AS, Pariente J, Barbeau EJ, Payoux P and Péran P. Insight on AV-45 binding in white and grey matter from histogram analysis: a study on early Alzheimer's disease patients and healthy subjects. Eur J Nucl Med Mol Imaging 2014; 41: 1408-1418.
[66] Heurling K, Buckley C, Vandenberghe R, Laere KV and Lubberink M. Separation of β-amyloid binding and white matter uptake of 18F-flutemetamol using spectral analysis. Am J Nucl Med Mol Imaging 2015; 5: 515-26.
[67] Fodero-Tavoletti MT, Rowe CC, McLean CA, Leone L, Li QX, Masters CL, Cappai R and Villemagne VL. Characterization of PiB binding to white matter in Alzheimer disease and other dementias. J Nucl Med 2009; 50: 198-204.
[68] Stankoff B, Freeman L, Aigrot MS, Chardain A, Dollé F, Williams A, Galanaud D, Armand L, Lehericy S, Lubetzki C, Zalc B and Bottlaender M. Imaging central nervous system myelin by positron emission tomography in multiple sclerosis using [methyl-11C]-2-(4'-methylaminophenyl)-6-hydroxybenzothiazole. Ann Neurol 2011; 69: 673-680.
[69] Villemagne VL, Mulligan RS, Pejoska S, Ong K, Jones G, O'Keefe G, Chan JG, Young K, Tochon-Danguy H, Masters CL and Rowe CC. Comparison of 11C-PiB and 18F-florbetaben for Abeta imaging in ageing and Alzheimer's disease. Eur J Nucl Med Mol Imaging 2012; 39: 983-989.
[70] Richards D and Sabbagh MN. Florbetaben for PET imaging of beta-amyloid plaques in the brain. Neurol Ther 2014; 3: 79-88.
[71] Chen CD, McCullough A, Gordon B, Joseph-Mathurin N, Flores S, McKay NS, Hobbs DA, Hornbeck R, Fagan AM, Cruchaga C, Goate AM, Perrin RJ, Wang G, Li Y, Shi X, Xiong C, Pontecorvo MJ, Klein G, Su Y, Klunk WE, Jack C, Koeppe R, Snider BJ, Berman SB, Roberson ED, Brosch J, Surti G, Jiménez-Velázquez IZ, Galasko D, Honig LS, Brooks WS, Clarnette R, Wallon D, Dubois B, Pariente J, Pasquier F, Sanchez-Valle R, Shcherbinin S, Higgins I, Tunali I, Masters CL, van Dyck CH, Masellis M, Hsiung R, Gauthier S, Salloway S, Clifford DB, Mills S, Supnet-Bell C, McDade E, Bateman RJ and Benzinger TLS; DIAN-TU Study Team. Longitudinal head-to-head comparison of 11C-PiB and 18F-florbetapir PET in a Phase 2/3 clinical trial of anti-amyloid-β monoclonal antibodies in dominantly inherited Alzheimer's disease. Eur J Nucl Med Mol Imaging 2023; 50: 2669-2682.
[72] Choi SR, Golding G, Zhuang Z, Zhang W, Lim N, Hefti F, Benedum TE, Kilbourn MR, Skovronsky D and Kung HF. Preclinical properties of 18F-AV-45: a PET agent for Aβ plaques in the brain. J Nucl Med 2009; 50: 1887-1894.
[73] Camus V, Payoux P, Barré L, Desgranges B, Voisin T, Tauber C, La Joie R, Tafani M, Hommet C, Chételat G, Mondon K, de La Sayette V, Cottier JP, Beaufils E, Ribeiro MJ, Gissot V, Vierron E, Vercouillie J, Vellas B, Eustache F and Guilloteau D. Using PET with 18F-AV-45 (florbetapir) to quantify brain amyloid load in a clinical environment. Eur J Nucl Med Mol Imaging 2012; 39: 621-631.
[74] Villemagne VL, Ong K, Mulligan RS, Holl G, Pejoska S, Jones G, O'Keefe G, Ackerman U, Tochon-Danguy H, Chan

JG, Reininger CB, Fels L, Putz B, Rohde B, Masters CL and Rowe CC. Amyloid imaging with 18F-florbetaben in Alzheimer disease and other dementias. J Nucl Med 2011; 52: 1210-1217.

[75] Abrahamson EE, Kofler JK, Becker CR, Price JC, Newell KL, Ghetti B, Murrell JR, McLean CA, Lopez OL, Mathis CA, Klunk WE, Villemagne VL and Ikonomovic MD. 11C-PiB PET can underestimate brain amyloid-beta burden when cotton wool plaques are numerous. Brain 2022; 145: 2161-2176.

[76] Ikonomovic MD, Klunk WE, Abrahamson EE, Mathis CA, Price JC, Tsopelas ND, Lopresti BJ, Ziolko S, Bi W, Paljug WR, Debnath ML, Hope CE, Isanski BA, Hamilton RL and DeKosky ST. Post-mortem correlates of in vivo PiB-PET amyloid imaging in a typical case of Alzheimer's disease. Brain 2008; 131: 1630-1645.

[77] Sperling RA, Laviolette PS, O'Keefe K, O'Brien J, Rentz DM, Pihlajamaki M, Marshall G, Hyman BT, Selkoe DJ, Hedden T, Buckner RL, Becker JA and Johnson KA. Amyloid deposition is associated with impaired default network function in older persons without dementia. Neuron 2009; 63: 178-188.

[78] Mason NS, Mathis CA and Klunk WE. Positron emission tomography radioligands for in vivo imaging of Abeta plaques. J Labelled Comp Radiopharm 2013; 56: 89-95.

[79] Rowe C, Pike K, Ng S, Savage G, Browne W, Ackermann U, Gong S, Chan G, O'Keefe G and Tochon-Danguy H. Aβ burden correlates with memory impairment in non-demented subjects but plateaus in established Alzheimer's disease: a PIB-PET cross sectional study. 2007.

[80] Lockhart SN, Schaich CL, Craft S, Sachs BC, Rapp SR, Jung Y, Whitlow CT, Solingapuram Sai KK, Cleveland M, Williams BJ, Burke GL, Bertoni A, Hayden KM and Hughes TM. Associations among vascular risk factors, neuroimaging biomarkers, and cognition: preliminary analyses from the Multi-Ethnic Study of Atherosclerosis (MESA). Alzheimers Dement 2022; 18: 551-560.

[81] Wong DF, Rosenberg PB, Zhou Y, Kumar A, Raymont V, Ravert HT, Dannals RF, Nandi A, Brašić JR, Ye W, Hilton J, Lyketsos C, Kung HF, Joshi AD, Skovronsky DM and Pontecorvo MJ. In vivo imaging of amyloid deposition in Alzheimer disease using the radioligand 18F-AV-45 (flobetapir F 18). J Nucl Med 2010; 51: 913-920.

[82] Montine TJ, Phelps CH, Beach TG, Bigio EH, Cairns NJ, Dickson DW, Duyckaerts C, Frosch MP, Masliah E, Mirra SS, Nelson PT, Schneider JA, Thal DR, Trojanowski JQ, Vinters HV and Hyman BT; National Institute on Aging; Alzheimer's Association. National Institute on Aging-Alzheimer's Association guidelines for the neuropathologic assessment of Alzheimer's disease: a practical approach. Acta Neuropathol 2012; 123: 1-11.

[83] Hyman BT, Phelps CH, Beach TG, Bigio EH, Cairns NJ, Carrillo MC, Dickson DW, Duyckaerts C, Frosch MP, Masliah E, Mirra SS, Nelson PT, Schneider JA, Thal DR, Thies B, Trojanowski JQ, Vinters HV and Montine TJ. National Institute on Aging-Alzheimer's Association guidelines for the neuropathologic assessment of Alzheimer's disease. Alzheimers Dement 2012; 8: 1-13.

[84] Ferrari C and Sorbi S. The complexity of Alzheimer's disease: an evolving puzzle. Physiol Rev 2021; 101: 1047-1081.

[85] Zhao Q, Du X, Chen W, Zhang T and Xu Z. Advances in diagnosing mild cognitive impairment and Alzheimer's disease using (11)C-PIB-PET/CT and common neuropsychological tests. Front Neurosci 2023; 17: 1216215.